ELSEVIER

Chemical Engineering Journal 78 (2000) 5–11

Chemical Engineering Journal

www.elsevier.com/locate/cej

Transient three-dimensional numerical analyses of shallow bubble column

Kenya Kuwagi, Sunao Kusu, Hiroyuki Ozoe*

Institute of Advanced Material Study, Kyushu University, Kasuga, Fukuoka 816, Japan

Received 9 November 1998; received in revised form 2 August 1999; accepted 16 August 1999

Abstract

Two-phase flow in a shallow bubble column (radius equal to the height) was studied. The primary objectives were to study both the effect of the free surface on the whole flow mode and the three-dimensionality in the whole domain. Air bubbles were injected through a central porous bottom wall of a cylindrical water tank. The flow pattern was visualized with dispersed aluminium particles. The velocity of the liquid phase was measured with a laser-Doppler velocimeter. The system was numerically analysed with a dispersed flow model. The inertial terms in the momentum equations were approximated by the QUICK scheme. Two models for the top surface were employed, namely either slip or non-slip conditions. The computed result with non-slip conditions agreed fairly well with the experimental result. A three-dimensional calculation was carried out with non-slip conditions for the top water surface. The calculated flow pattern agreed better with the experimental pattern than the two-dimensional calculation. In the results, two spiral vortices moving vertically were found outside the central upward flow. The flow was strongly three-dimensional, even though the vessel was shallow.

Keywords: Gas–liquid two-phase flow; Bubble column; Dispersed flow model; Three-dimensional analysis; Numerical analysis; Free surface

1. Introduction

Gas–liquid two-phase flow problems arise in many industrial processes and have been analysed in various fields of engineering.

A two-phase flow in a vessel usually has a free surface. A variable height or shape of the liquid in a vessel with a free surface has been considered in many reports (e.g., Ref. [1]). However, there appear to be few reports which have considered the purity of the liquid. A free surface of even a slightly contaminated liquid is similar to a solid wall [2]. It is well known that the terminal velocity of an ascending bubble in a pure static liquid is different from that in a contaminated liquid as an example of this effect. As discussed by Bernal et al. [3], the capillary stress in a boundary layer at the top surface is balanced by the viscous stress and this is also the case at the bubble surface.

In a large and/or deep vessel, a bubble plume often sways and the flow is unsteady and/or three-dimensional. Many papers concerning such a flow have been reported. Becker et al. [4] carried out a calculation and experiment for unsteady two-dimensional gas–liquid flow in rectangular bubble columns with good agreement between them. We also studied such a flow in a vertical cylinder and obtained oscillatory flow patterns [5]. However, there are few reports about the flow in a shallow vessel. Thus the flow is often considered to be almost two-dimensional and axisymmetric in a cylinder.

In this paper, both numerical and experimental analyses were carried out for the two-phase flow problems in a shallow vertical cylinder. Two models for the top surface were considered, namely either slip or non-slip conditions. Furthermore, a three-dimensional model was employed.

2. Experimental details

The experimental set-up is shown schematically in Fig. 1. The inner radius of the acrylic cylinder is 80 mm. The cylinder was filled with tap water to a height of 80 mm. Air bubbles were injected through the central porous bottom wall of the cylinder into a water tank with a mass flow rate $Q=1.67\times10^{-6}\,m^3\,s^{-1}$. This gas rate and, hence, gas hold-up is relatively low compared with that used in a practical bubble column. Such a low gas hold-up is often utilized in a bubble column for wastewater treatment and biological processes. The standard maximum diameter of the hole is 100–150 μm and $r_c=10$ mm.

Firstly, to understand the whole flow pattern, aluminium particles were dispersed into water which was then illuminated by a slit light from a projector. In order to obtain better visualization, the cylinder was surrounded by a square

* Corresponding author. Tel.: +81-92-583-7834; fax: +81-92-583-7838.
E-mail address: ozoe@cm.kyushu-u.ac.jp (H. Ozoe)

1385-8947/00/$ – see front matter
PII: S1385-8947(99)00154-0

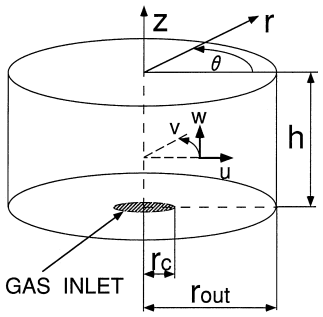

Fig. 1. Problem Schematic diagram of experimental set-up.

acrylic box, and tap water was filled in between. Flow patterns were taken by a camera, with a shutter speed of 1 s.

Secondly, the velocity profile of the liquid phase was measured by a laser-Doppler velocimeter (LDV) with a forward scattering method. Data samples of 256 pieces were taken at each point.

3. Theoretical analyses

For numerical analysis, the following assumptions were utilized:

1. mass transfer between the liquid and gas phases does not exist;
2. the liquid and gas phases are treated as incompressible fluids;
3. the temperature in the domain is constant and uniform;
4. coalescence and fragmentation of the bubbles are not considered;
5. no turbulence models are employed.

From the above assumptions, the governing equations become as follows.

3.1. Continuity equations

k=G (gas phase), L (liquid phase)

$$\frac{\partial \varepsilon_k}{\partial t} + \nabla \cdot (\varepsilon_k \boldsymbol{v}_k) = 0 \tag{1}$$

$$\varepsilon_L + \varepsilon_G = 0 \tag{2}$$

The summation of two equations with k=G and L in Eq. (1) leads to Eq. (3) by considering Eq. (2) [6]. This equation does not have any time-dependent terms.

$$\nabla \cdot (\varepsilon_G \boldsymbol{v}_G) + \nabla \cdot (\varepsilon_L \boldsymbol{v}_L) = 0 \tag{3}$$

3.2. Dispersed flow model

In this numerical analysis, a dispersed flow model [7] was adopted. The model equations for a dispersed flow are as follows:

momentum equation for a liquid phase

$$\varepsilon_L \rho_L \frac{D_L \boldsymbol{v}_L}{Dt} = -\varepsilon_L \nabla p + \varepsilon_L \boldsymbol{F}_V + \boldsymbol{F}_D + \boldsymbol{F}_L - \rho_L g \varepsilon_L \tag{4}$$

momentum equation for a gas phase

$$\varepsilon_G \rho_G \frac{D_G \boldsymbol{v}_G}{Dt} = -\boldsymbol{F}_D - \boldsymbol{F}_L + (\rho_L - \rho_G) g \varepsilon_G \tag{5}$$

where D_k/Dt is the material derivative following phase k.

3.3. Interfacial force

(1) Viscous force: the viscous force $\boldsymbol{F}_V$ is expressed as shown in Appendix with μ. Here μ is the apparent viscosity for a bubbly flow. Following Taylor [8], the following equation was employed

$$\mu = \mu_L (1 + \varepsilon_G) \tag{6}$$

(2) Drag force

$$\boldsymbol{F}_D = \frac{3}{4} \frac{C_D \varepsilon_G \rho_L \boldsymbol{v}_r |\boldsymbol{v}_r|}{d_B} \tag{7}$$

where C_D is the drag coefficient and the following relation of Stokes and Schiller–Naumann was used.

$$C_D = \begin{cases} 24/\mathrm{Re} & \mathrm{Re} \le 2 \\ (24/\mathrm{Re})\,(1 + 0.15\mathrm{Re}^{0.687}) & \mathrm{Re} \ge 2 \end{cases} \tag{8}$$

where Re is the bubble Reynolds number, $\mathrm{Re}=\rho_L d_B \boldsymbol{v}_r/\mu_L$, d_B is the bubble diameter and $\boldsymbol{v}_r$ is the relative velocity ($=\boldsymbol{v}_G - \boldsymbol{v}_L$); d_B was set to 2.0 mm.

(3) Lift force [9]

$$\boldsymbol{F}_L = C_L \rho_L \varepsilon_G \boldsymbol{v}_r \times (\nabla \times \boldsymbol{v}_L) \tag{9}$$

where C_L is the lift force coefficient. C_L was set to a constant value: 0.2 by Ref. [5].

3.4. Numerical procedure

The above momentum equations were approximated by finite difference equations. Time discretization was approximated by an explicit method and inertial terms by the QUICK scheme [10]. The pressure distribution was solved with the HS-MAC method.

The initial conditions are as follows. The liquid is static and no bubbles exist in the cylinder.

Table 1
Calculation conditions

No.	Grid numbers			Top surface
	r	θ	z	
1	24	–	24	Non-slip
2	40	–	40	Non-slip
3	96	–	80	Non-slip
4	120	–	120	Non-slip
5	96	–	80	Non-slip
6	96	–	80	Slip
7	40	36	40	Non-slip

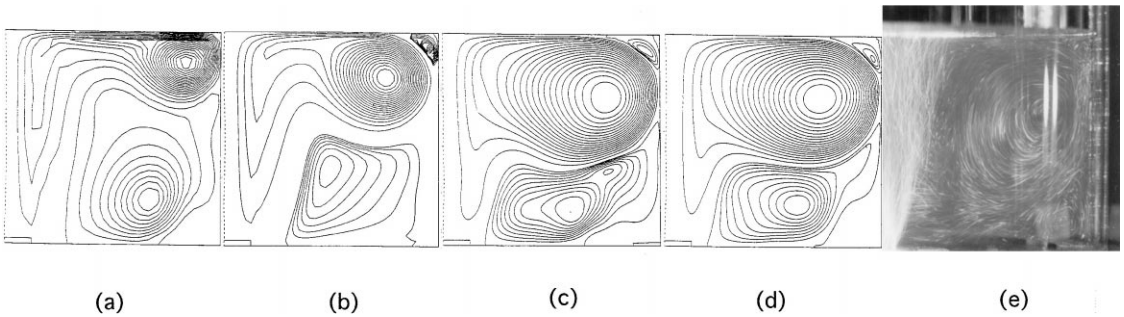

Fig. 2. The effect of the grid number on the stream lines of the liquid phase computed with a two-dimensional model: (a) 24×24; (b) 40×40; (c) 96×80; (d) 120×120; (e) photograph.

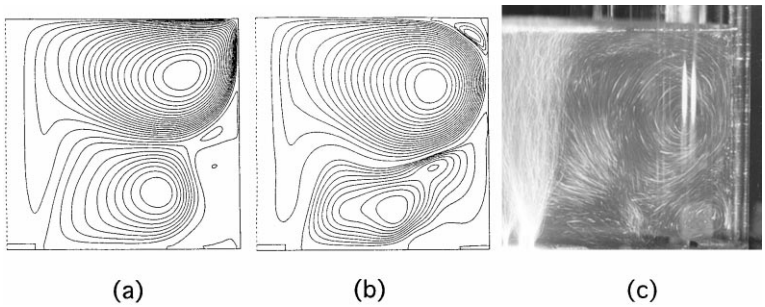

Fig. 3. Flow pattern of the liquid phase with different boundary conditions for the top surface: (a) slip conditions; (b) non-slip conditions; (c) photograph.

The boundary conditions are as follows:
liquid phase

wall : $u_L = v_L = w_L = 0$
top surface : free or rigid conditions

where the height of the liquid surface is assumed to be flat from the experimental observation, although a deformed surface was studied by Matsumoto and Murai [1];
gas phase

wall : slip conditions
top surface : bubbles leave from a free surface immediately

$$\left(\frac{\partial u_G}{\partial z} = \frac{\partial v_G}{\partial z} = \frac{\partial w_G}{\partial z} = \frac{\partial \varepsilon_G}{\partial z} = 0\right)$$

The calculation conditions are shown in Table 1.

4. Results and discussion

4.1. Effect of grid number

Fig. 2 shows the effect of the grid number on the stream lines of the liquid phase computed with a two-dimensional model (cases 1–4 in Table 1). Upward flow caused by ascending bubbles in the central region makes a large vortex (main vortex) in the vertical section. The main vortex calculated with coarse grids (Figs. 2a and b) is small. The main vortex computed using a higher order upwind scheme with a coarse grid is sometimes smaller than the real one for high

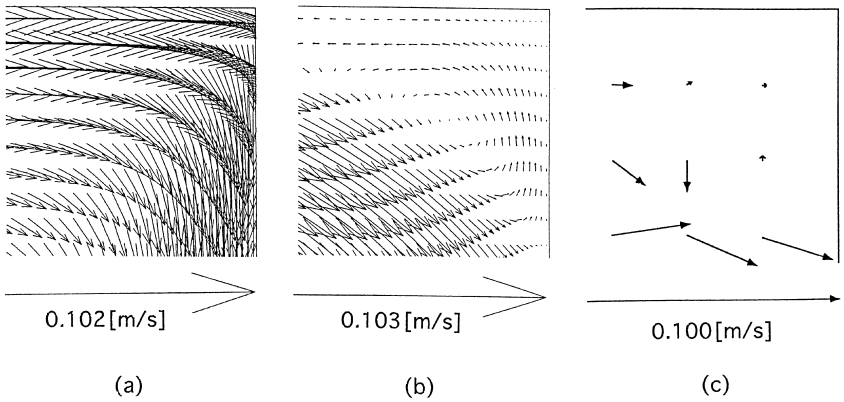

Fig. 4. Magnification of the top right-hand corner of Fig. 3: (a) slip conditions; (b) non-slip conditions; (c) experimental result with LDV.

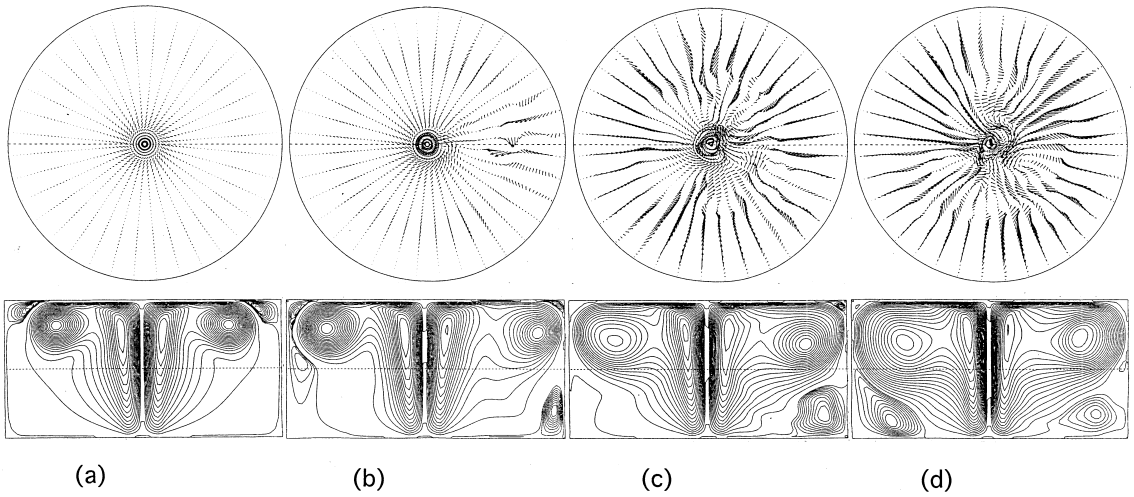

Fig. 5. A series of instantaneous velocity vectors in the horizontal section at z/h=0.5 and those of the circumferential vector potential component in the vertical section: (a) t=6.55 s; (b) t=13.1 s; (c) t=19.6 s; (d) t=26.2 s.

Re number flow [11]. On the other hand, the sizes of the main vortices in Fig. 2c and d are almost the same. Therefore, the grid number 96×80 appears to be sufficient for this problem.

4.2. Boundary condition at the top surface

Chu et al. [2] reported that the flow near a slightly contaminated free surface is similar to that with a solid top surface in a single-phase flow problem.

Fig. 3 shows the flow pattern of the liquid phase with slip conditions (a) and with non-slip conditions (b) for the top surface (cases 5 and 6 in Table 1). A small vortex (secondary vortex) can be seen in the top right-hand corner in Fig. 3b. This can be seen in the photograph, but not in the calculated flow pattern with slip conditions. This tendency agrees with that obtained by Chu et al. [2].

Fig. 4 shows a magnification of the top right-hand corner of Fig. 3. The size of the secondary vortex calculated with non-slip conditions is almost the same as the experimental value. In this experiment, tap water was used, which is usually considered to be contaminated. Chu et al. [2] and Bernal et al. [3] explained that the advection of surface active agents by a vortex motion underneath can generate capillary stresses at the surface that must be balanced by viscous stresses in a boundary layer at the free surface. Tryggvason et al. [12] have carried out calculations considering the effect of the amount of surface contaminant. However, it was difficult to obtain a value for the contaminant. Therefore, non-slip conditions are effective and convenient for this problem, even though they may not be exact.

4.3. Three-dimensional analysis

Fig. 5 shows a series of instantaneous velocity vectors in the horizontal section at z/h=0.5 and those of the circumferential vector potential component in the vertical section with a three-dimensional model (case 7 in Table 1). From this figure, the size of the main vortex increases as the circumferential flow develops. Furthermore, the obliquely descending flow towards the bottom of the vessel can be

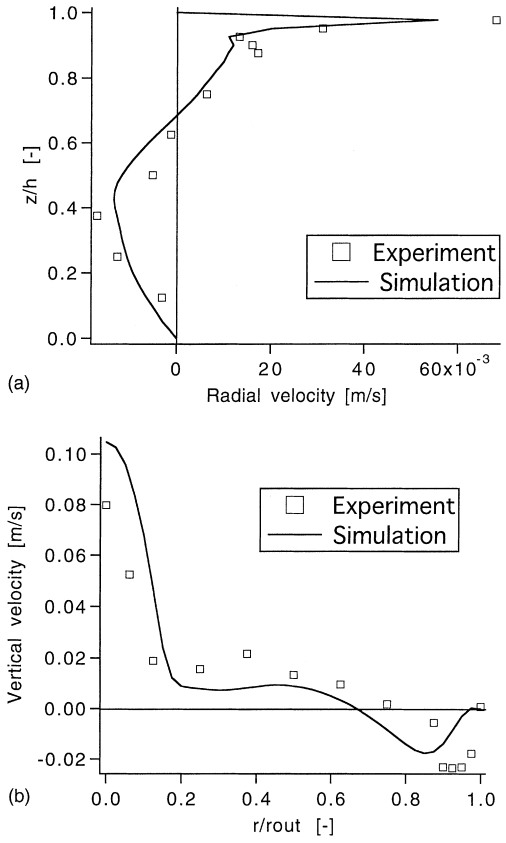

Fig. 6. Time averaged velocity distribution of liquid phase: (a) vertical distribution of the radial velocity along r/r_{out}=0.5; (b) radial distribution of the vertical velocity along z/h=0.5.

seen after the flow develops sufficiently in Fig. 5c and d. This flow was not obtained by a two-dimensional calculation. Accordingly, this obliquely descending flow would be caused by a downward flow in the θ–z section.

Fig. 6 shows both experimental and calculated velocity distributions of the liquid phase. Fig. 6a shows the vertical distribution of the radial velocity component along the vertical line at r/r_{out}=0.5, and Fig. 6b shows the radial distribution of the velocity component along the radial line at z/h=0.5. The data represent the value averaged over 256 samples in the experiment or 240 samples in the calculation, over a certain time period at each point. The periods are 13.1 s in the calculated results and about 10–20 s in the experimental results, depending on the particle sampling conditions. The calculated profiles agree reasonably with the experimental ones. In particular, good agreement can be seen near the top surface approximated with non-slip conditions in Fig. 6a.

4.4. Unsteady analysis of developed flow

Fig. 7 shows a series of instantaneous short time streak lines from 30×30 points in the vertical section. The length of each line corresponds to the motion of a particle which can move at the same speed as the liquid flow for 1 s. This term agrees with the shutter speed of the camera. An experimental photograph is shown in Fig. 7h. Here, the calculated streak lines do not exactly correspond to the experimental path lines. From this figure, the size and location of the main vortices change at every moment. Moreover, the descending flow in the lower part of the main vortices extends and shrinks alternately.

Fig. 8 shows multiple streak lines around a central upward flow region. The small circles in this figure represent the terminal points. Two vertical spiral flows can be seen around the central upward flow. The streak lines in the left spiral flow are denser than those in the right. This means that the upward velocity of the left spiral flow is smaller than that of the right. Such a vertical spiral flow appeared every second, though the numbers and locations changed with time. It is difficult to describe such a flow with velocity vectors or shorter term streak lines in a horizontal section like Fig. 7. We have not seen any previous reports that have described such vertical spiral flows. As seen in the photograph of Fig. 7h, the flow is almost axisymmetric. From such a photograph, the flow of this system may be considered to be two-dimensional.

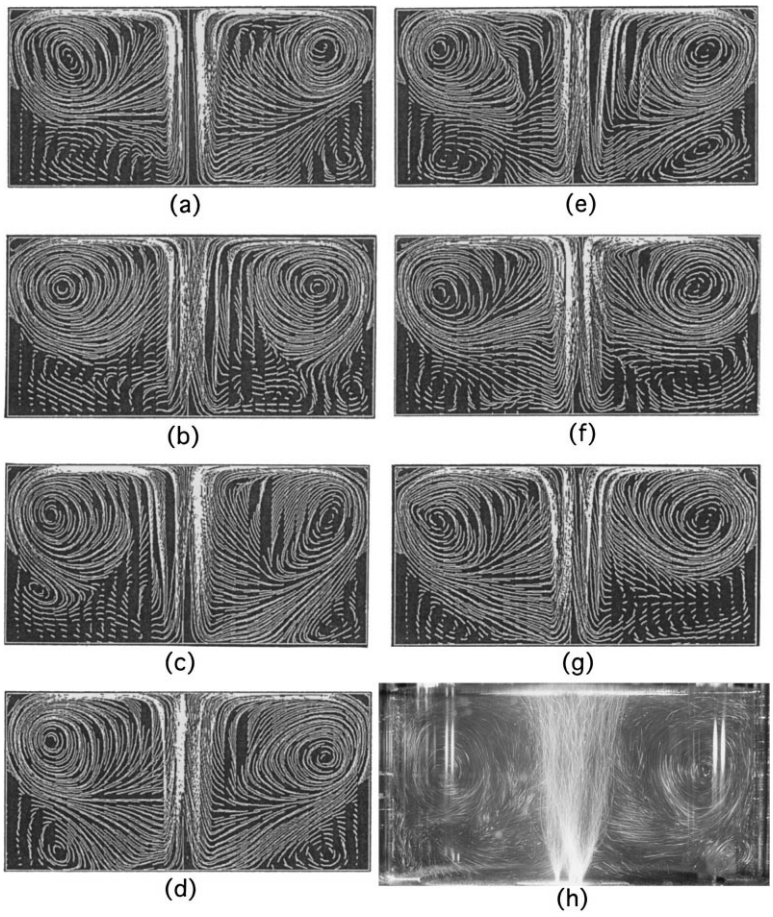

Fig. 7. A series of instantaneous streak lines from 30×30 points in the vertical section (Δt=1.0 s): (a) t=26.2 s; (b) t=29.5 s; (c) t=32.7 s; (d) t=36.0 s; (e) t=39.3 s; (f) t=42.6 s; (g) t=45.8 s; (h) photograph.

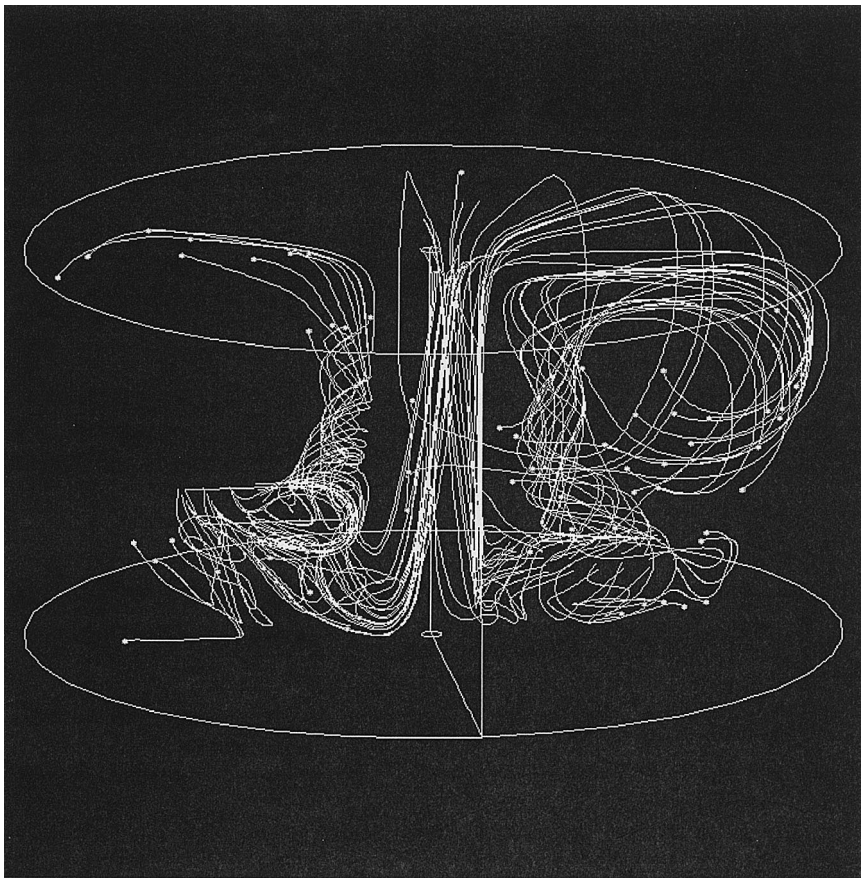

Fig. 8. Streak lines of liquid flow just outside a central rising bubble plume. Small circles are terminal points.

However, the flow of the liquid phase appears to be strongly three-dimensional as seen in Fig. 8. Nevertheless, the gas phase is almost axisymmetric, because the water height is low compared with the upward velocity of the gas phase (about 0.2 m s^{-1}). The streak lines of the gas phase based on the gas velocity (not shown due to space limitation) arrive at the top surface almost linearly in spite of this complicated convection of the liquid phase.

Two opposite results, i.e. a three-dimensional spiral liquid flow and an almost axisymmetric gas flow, appear to be useful to explain the structure of bubble plumes swaying in a deep and/or large vessel. Bubble plumes also sway slightly in this flow, although it is not clear because of the shallow vessel. This may be affected by such spiral flows.

5. Conclusions

Two-phase flow in a shallow vertical cylinder was investigated numerically and experimentally. The following conclusions were obtained.

1. An obliquely descending flow towards the centre bottom of the vessel was observed in the visualized result. Three-dimensional numerical analyses successfully simulated this flow.
2. The calculated result with non-slip conditions at the top surface agreed fairly well with the experimental result. Non-slip conditions for a free top surface are more appropriate than slip conditions for this problem with tap water.
3. Streak lines from multiple points represent a detailed flow mode including two spiral vortices moving vertically just outside the central bubble plume.

Although the present system may be presumed to be almost axisymmetric and two-dimensional because the vessel is small and shallow, the flow is, in fact, strongly three-dimensional and the circumferential velocity component is quite dominant for this problem.

6. Nomenclature

C_D	drag coefficient
C_L	lift force coefficient
d_B	diameter of a bubble (m)
$\boldsymbol{F}_D$	drag force per unit volume (N m^{-3})
$\boldsymbol{F}_L$	lift force per unit volume (N m^{-3})
$\boldsymbol{F}_V$	shear force per unit volume (N m^{-3})
g	gravitational acceleration (m s^{-2})
h	height of liquid surface (m)

p	pressure (Pa)
Q	injected gas flow rate ($m^3\,s^{-1}$)
r	radial coordinate (m)
r_c	radius of gas injection porous plate (m)
Re	Reynolds number ($=\rho_L d_B \boldsymbol{v}_r/\mu_L$)
r_{out}	radius of vessel (m)
t	time (s)
u	radial velocity component ($m\,s^{-1}$)
$\boldsymbol{v}$	velocity vector ($m\,s^{-1}$)
v	circumferential velocity component ($m\,s^{-1}$)
$\boldsymbol{v}_r$	slip velocity ($=\boldsymbol{v}_G-\boldsymbol{v}_L$) ($m\,s^{-1}$)
w	vertical velocity component ($m\,s^{-1}$)
z	vertical coordinate (m)

Greek letters

ε	void fraction (gas hold-up) (-)
θ	circumferential coordinate (rad)
μ	viscosity (Pa s)
ρ	density ($kg\,m^{-3}$)

Subscript

G	gas phase
k	gas phase (k=G) or liquid phase (k=L)
L	liquid phase

Operator

$D/Dt=\partial/\partial t+\boldsymbol{v}_k\cdot\nabla$

Appendix

The viscous force $\boldsymbol{F}_V$ which includes the variable viscosity is expressed for each component of cylindrical coordinates as follows:

r-component

$$\boldsymbol{F}_{V,r} = -\left\{\frac{1}{r}\frac{\partial}{\partial r}(r\tau_{rr}) + \frac{1}{r}\frac{\partial \tau_{r\theta}}{\partial \theta} - \frac{\tau_{\theta\theta}}{r} + \frac{\partial \tau_{rz}}{\partial z}\right\} \quad \text{(A1)}$$

θ-component

$$\boldsymbol{F}_{V,\theta} = -\left\{\frac{1}{r^2}\frac{\partial}{\partial r}(r^2\tau_{r\theta}) + \frac{1}{r}\frac{\partial \tau_{\theta\theta}}{\partial \theta} + \frac{\partial \tau_{\theta z}}{\partial z}\right\} \quad \text{(A2)}$$

z-component

$$\boldsymbol{F}_{V,z} = -\left\{\frac{1}{r}\frac{\partial}{\partial r}(r\tau_{rz}) + \frac{1}{r}\frac{\partial \tau_{\theta z}}{\partial \theta} + \frac{\partial \tau_{zz}}{\partial z}\right\} \quad \text{(A3)}$$

where τ is a stress tensor and expressed as follows:

$$\tau_{rr} = -\mu\left\{2\frac{\partial u}{\partial r} - \frac{2}{3}(\nabla\cdot\boldsymbol{v})\right\} \quad \text{(A4)}$$

$$\tau_{\theta\theta} = -\mu\left\{2\left(\frac{1}{r}\frac{\partial v}{\partial \theta} + \frac{u}{r}\right) - \frac{2}{3}(\nabla\cdot\boldsymbol{v})\right\} \quad \text{(A5)}$$

$$\tau_{zz} = -\mu\left\{2\frac{\partial w}{\partial z} - \frac{2}{3}(\nabla\cdot\boldsymbol{v})\right\} \quad \text{(A6)}$$

$$\tau_{r\theta} = \tau_{\theta r} = -\mu\left\{r\frac{\partial}{\partial r}\left(\frac{v}{r}\right) + \frac{1}{r}\frac{\partial u}{\partial \theta}\right\} \quad \text{(A7)}$$

$$\tau_{\theta z} = \tau_{z\theta} = -\mu\left\{\frac{\partial v}{\partial z} + \frac{1}{r}\frac{\partial w}{\partial \theta}\right\} \quad \text{(A8)}$$

$$\tau_{zr} = \tau_{rz} = -\mu\left\{\frac{\partial w}{\partial r} + \frac{\partial u}{\partial z}\right\} \quad \text{(A9)}$$

References

[1] Y. Matsumoto, Y. Murai, Trans. Jpn. Soc. Mech. Eng. Ser. B 61 (1995) 2818.
[2] C.C. Chu, C.T. Wang, C.S. Hsieh, Phys. Fluid A 5 (1993) 662.
[3] L.P. Bernal, A. Sokolichin, G. Eigenberger, Phys. Fluid A 1 (1994) 2001.
[4] S. Becker, A. Sokolichin, G. Eigenberger, Chem. Eng. Sci. 49 (1994) 5747.
[5] K. Kuwagi, H. Ozoe, Proceeding of International Conference on Fluid and Thermal Energy, Yogyakarta, Indonesia (1997) 389.
[6] A. Tomiyama, I. Kataoka, T. Ohkawa, M. Hirano, Trans. Jpn. Soc. Mech. Eng. Ser. B 59 (1993) 3003.
[7] I. Kataoka, A. Tomiyama, Jpn J. Multiphase Flow 7 (1993) 132.
[8] G.I. Taylor, Proc. Roy. Soc. A138 (1932) 41.
[9] D.A. Drew, R.T. Lahey, Int. J. Multiphase Flow 13 (1987) 113.
[10] B.P. Leonard, Comp. Methods Appl. Mech. Eng. 19 (1979) 59.
[11] K. Kuwagi, H. Ozoe, Kagaku Kogaku Ronbunshu 23 (1997) 861.
[12] G. Tryggvason, J. Abdollahi-Alibeik, W.W. Willmarth, A. Hirsa, Phys. Fluid A 4 (1992) 1215.